Supplement of Atmos. Chem. Phys., 19, 8063–8081, 2019
https://doi.org/10.5194/acp-19-8063-2019-supplement
© Author(s) 2019. This work is distributed under
the Creative Commons Attribution 4.0 License.

Atmospheric Chemistry and Physics
Open Access
EGU

Supplement of

Significant source of secondary aerosol: formation from gasoline evaporative emissions in the presence of SO_2 and NH_3

Tianzeng Chen et al.

Correspondence to: Qingxin Ma (qxma@rcees.ac.cn) and Hong He (honghe@rcees.ac.cn)

The copyright of individual parts of the supplement might differ from the CC BY 4.0 License.

S1. AMS Corrections: Comparison with SMPS Measurements

Theoretically, the sum of the secondary aerosol (SA) mass measured by HR-ToF-AMS should be equal to the mass calculated from the SMPS size distributions. However, both methods have their limitations, in which SMPS measures particle mobility diameter, while HR-ToF-AMS measures mass. Therefore, particle shape and density must be assumed before converting SMPS measurements to mass. Here, we assume that particles are spherical, and the density of SA were calculated from the equation $\rho = d_{va}/d_m$, where d_{va} is the mean vacuum aerodynamic diameter measured by an HR-ToF-AMS and d_m is the mean electrical mobility diameter measured by SMPS (DeCarlo et al., 2004). However, fractal-like particles will cause the SMPS to overestimate the spherical equivalent diameter and therefore overestimate the particle mass. While, HR-ToF-AMS tends to underestimate the SA mass due to the transmission efficiency (Liu et al., 2007) and collection efficiency (Takegawa et al., 2005).

For all the experiments with the discrepancies between HR-ToF-AMS and SMPS, we assume that the difference in mass has the same chemical composition as the measured chemical species (i.e., organics, nitrate, sulfate, and ammonium). And then a scaling factor (AMS_{sf}) was calculated for each experiment to correct the SA mass measured by HR-ToF-AMS and close the gap with the SMPS measurement. The scaling factor could be calculated as following equation:

$$AMS_{sf} = \frac{C_{SMPS}}{C_{Org} + C_{NO_3} + C_{SO_4} + C_{NH_4}}$$

in which C_{SMPS} is the SA mass concentration derived from SMPS, C_{Org}, C_{NO_3}, C_{SO_4} and C_{NH_4} are the mass concentrations of organics, nitrate, sulfate, and ammonium measured by HR-ToF-AMS, respectively. The AMS_{sf} for each time step after wall loss correction is calculated and used to scale the AMS data for the entire experiment. For all the experiments the average AMS_{sf} ranged from 1.09 to

1.23.

S2. Vapor wall loss and gas-particle partitioning timescales

The loss of vapor by condensation onto the wall is generally considered to be a first-order process, which can be characterized by the first-order wall-loss coefficient k_w (s^{-1}). According to the following equation reported by McMurry and Grosjean (1985), the value of k_w is equal to:

$$k_w = \frac{A}{V} \times \frac{\alpha_w \bar{c}}{1.0 + \frac{\pi}{2} \times \left[\frac{\alpha_w \bar{c}}{4(k_e D_{gas})^{0.5}}\right]}$$

in which A and V are the surface and volume of the smog chamber, respectively. For our cuboid smog chamber (L × W × H = 3.0 × 2.5 × 4.0 m), A=59 m^2, V=30 m^3. α_w is the mass accommodation coefficient of vapors onto the chamber walls, $\bar{c}$ is the mean thermal speed of the molecules, k_e is the coefficient of eddy diffusion, and D_{gas} is the gas-phase diffusivity.

For a given vapor molecule, the mean thermal speed $\bar{c}$ could be calculated according to the following equation:

$$\bar{c} = \sqrt{\frac{8RT}{\pi MW}}$$

in which R is the ideal gas constant (i.e., 8.314 J mol^{-1} K^{-1}), T is the experimental temperature (T=299.15 K in this study), and MW is the molecular weight (an upper bound and a lower bound of molecular mass of organic vapors was adopted, i.e., 100 g mol^{-1} and 300 g mol^{-1} in this study).

D_{gas} is assumed to vary with molecular weight (MW) and is equal to $D_{CO_2}(MW_{CO_2}/MW)$, with D_{CO_2} = 1.38 × 10^{-5} m^2 s^{-1}. Therefore, this leaves k_e and α_w as the two key unknowns. For the value of k_e, 0.015 s^{-1} was estimated according to the values reported by previous studies for a 28 m^3 Caltech chamber (Loza et al., 2012; McMurry and Rader, 1985; Zhang et al., 2014). For the value of α_w, 10^{-5} was adopted

according to the experimental results of Matsunaga and Ziemann (2010).

Then the timescale associated with vapor-wall loss ($\tau_{g\text{-}w}$) is calculated to be:

$$\tau_{g-w} = k_w^{-1}$$

for the timescale associated with reaching gas-to-particle partitioning equilibrium ($\bar{\tau}_{g\text{-}p}$), which varies with particle number concentration and diameter, and could be approximately calculated to be:

$$\bar{\tau}_{g-p} = (2\pi N_p \overline{D_p} D_{gas} \overline{F_{FS}})^{-1}$$

in which N_p is the particle number concentration, $\overline{D_p}$ is the particle mean diameter, D_{gas} is the gas-phase diffusivity and $\overline{F_{FS}}$ is the correction to the mass transfer flux due to noncontinuum effects and imperfect accommodation given in the following equation:

$$\overline{F_{FS}} = \frac{0.75\alpha(1 + k_n)}{k_n^2 + k_n + 0.283 k_n \alpha + 0.75\alpha}$$

in which α is the mass accommodation coefficient onto particles, for which the value of 0.002 was adopted in this study, and k_n is the Knudsen number, defined as:

$$k_n = \lambda / R_p$$

in which λ is the gas mean free path, which could be calculated as following equation:

$$\lambda = \frac{3 D_{gas}}{\bar{c}}$$

In our study, the SA yields were underestimated by a factor of 1.97−2.82 fold when considering the ratio of these two timescales (i.e., $\bar{\tau}_{g\text{-}p}/\tau_{g\text{-}w}$), which showed a decreasing trend with increasing SO_2 and NH_3 initial concentrations, suggesting that an increasing proportion of vapors is partitioned onto the suspended particle surface rather than the chamber wall. Meanwhile, the wall loss of sulfuric acid gas was also considered using this ratio (i.e., $\bar{\tau}_{g\text{-}p}/\tau_{g\text{-}w}$) to correct the sink of sulfur species.

S3. Positive matrix factorization (PMF)

77 Positive Matrix Factorization (PMF) (Paatero, 1997; Paatero and Tapper, 1994) is a receptor model
78 and multivariate factor analysis tool that decomposes a matrix of speciated sample data into two matrices,
79 namely factor contributions and factor profiles. In recent years, the PMF model was used for the analysis
80 of high-resolution (HR) mass spectra data which can provide better separation of different organic
81 components (Liu et al., 2014). This model was expressed as a bilinear factor model, namely, $x_{ij}=\sum_p g_{ip}f_{pj}$
82 $+ e_{ij}$, where i and j refer to values of j species in i samples, respectively, p is the number of factors in the
83 solution, and used a least-squares fitting process, minimizing a quality of fit parameter. In our study, we
84 used the PMF software together with a modified version of the CU AMS PMF Execute Calcs Tool v
85 2.06, which was developed by Ulbrich et al. (2009), to analyze the HR mass spectra (*m/z* 12 – 170)
86 (Zhang et al., 2011). The data and noise matrices input into the PMF analysis were generated from the
87 PIKA version 1.15D. Ions were classified and down-weighted according to the signal-to-noise ratios
88 (SNR). 0.2<SNR<2 was classified as the weak ions and down-weighted by a factor of 2, SNR<0.2 was
89 bad ions and removed from the analysis and noise values of CO_2^+-related peaks at m/z 16 (O), 17 (HO),
90 18 (H_2O), 28 (CO), and 44 (CO_2) were down-weighted.

91 Table S1. The volume fraction of detected compounds for gasoline utilized in this study.

Compounds	Volume Fraction (v/v %)	Compounds	Volume Fraction (v/v %)
1,3-Butadiene	10.67	n-Octane	1.71
1-Pentene	0.00	p-Xylene and m-Xylene	2.28
trans-2-Pentene	0.06	Ethylbenzene	1.82
cis-2-Pentene	0.06	Nonane	0.75
Isoprene	1.33	o-Xylene	1.09
2,2-Dimethylbutane	1.11	Styrene	0.00
2,3-Dimethylbutane	7.74	Isopropylbenzene	0.30
2-Methylpentane	7.83	n-Propylbenzene	2.11
3-Methylpentane	5.63	1,3,5-Trimethylbenzene	0.93
1-Hexene	0.00	m-Ethyltoluene	0.93
n-Hexane	9.89	p-Ethyltoluene	0.93
2,4-Dimethylpentane	2.42	n-Decane	0.00
Methylcyclopentane	3.70	o-Ethyltoluene	0.60
Cyclohexane	1.91	1,2,4-Trimethylbenzene	5.12
2-Methylhexane	2.18	1,2,3-Trimethylbenzene	0.92
3-Methylhexane	2.62	m-Diethylbenzene	0.17
2,3-Dimethylpentane	2.53	p-Diethylbenzene	0.17
Benzene	0.58	n-Undecane	0.00
2,2,4-Trimethylpentane	3.87	n-Dodecane	0.83
n-Heptane	5.12		
Methylcyclohexane	2.43		
2,3,4-Trimethylpentane	1.20		
2-Methylheptane	0.62		
3-Methylheptane	0.59		
Toluene	4.90		

92

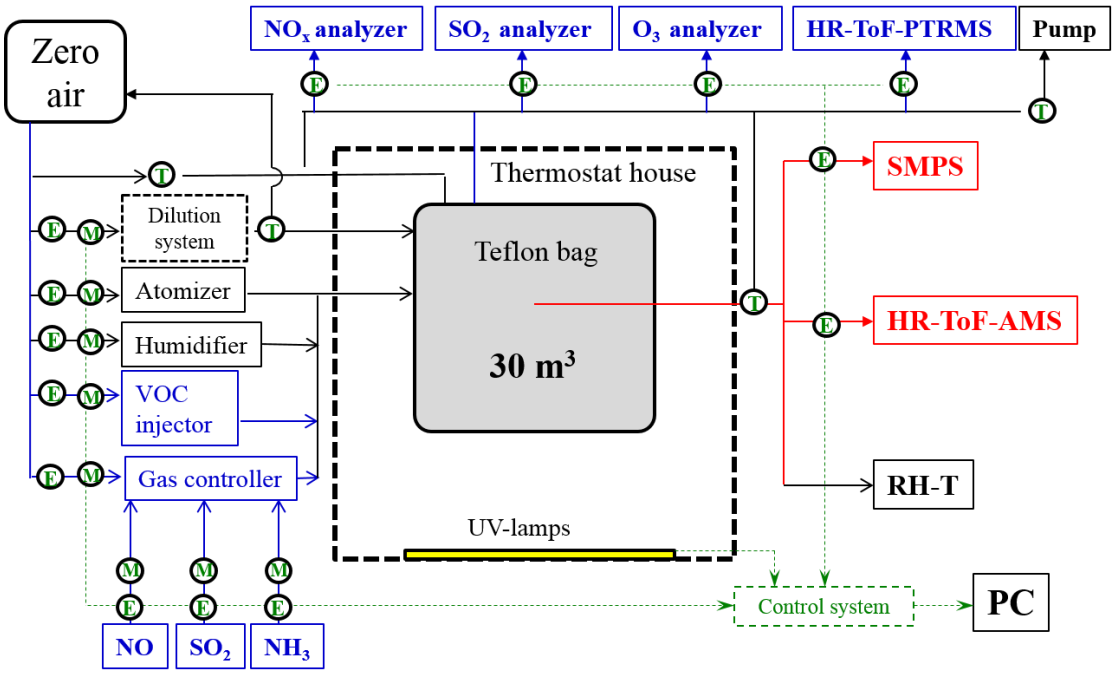

93

94 Fig. S1. Schematic of the RCEES-CAS smog chamber facility. E: Electromagnetic valve; T: Three-way valve. M:

95 Mass flow controller.

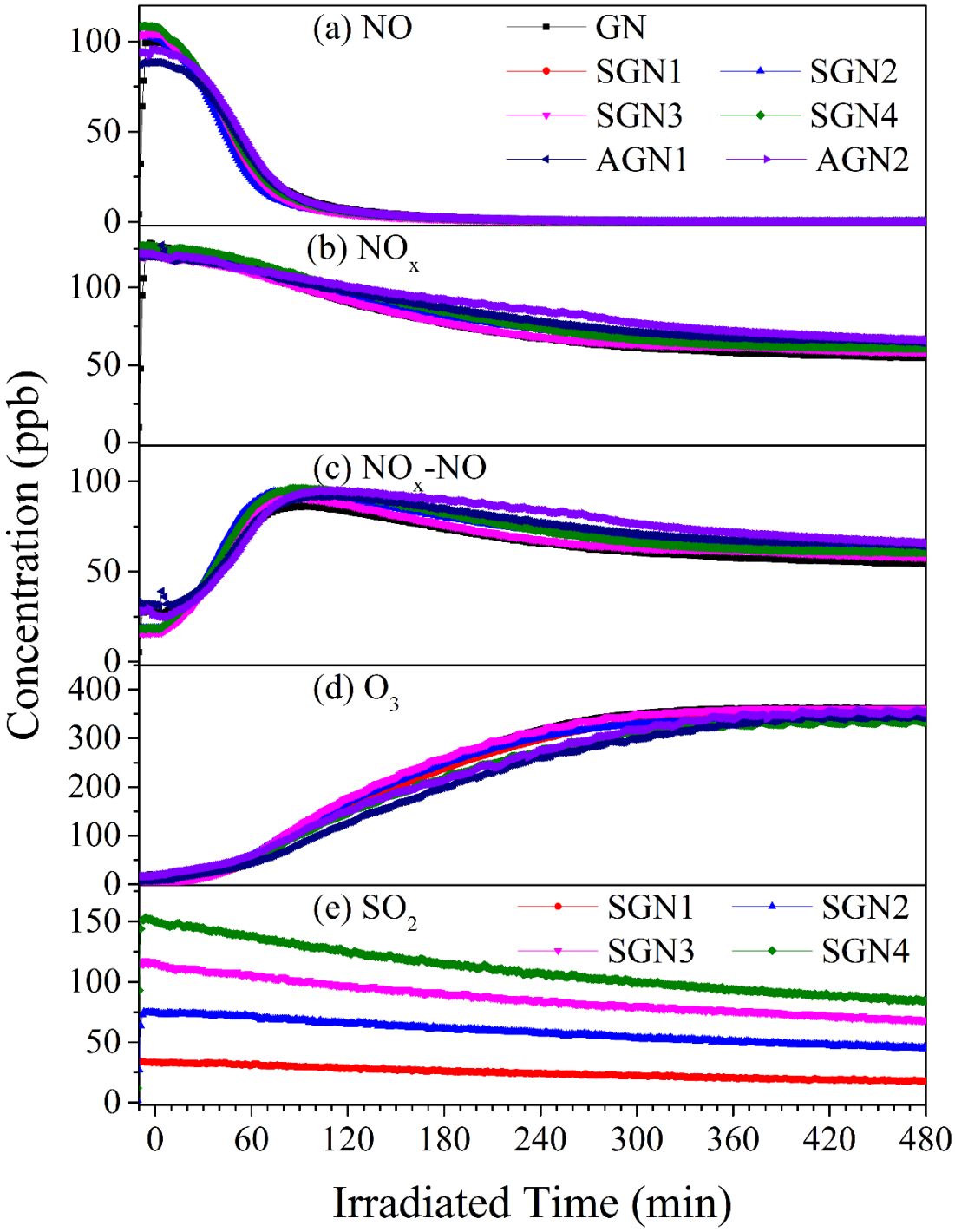

Fig. S2. Time variations of inorganic gas-phase species (a) NO, (b) NO_x, (c) NO_x-NO, (d) O_3, and (e) SO_2 in photo-oxidation of gasoline/NO_x in the presence or absence of SO_2 and NH_3. Letters in abbreviations represent the reactants introduced into the chamber reactor, i.e., "G" represents gasoline, "N" represents nitrogen oxides, "S" represents sulfur dioxide, "A" represents ammonia.

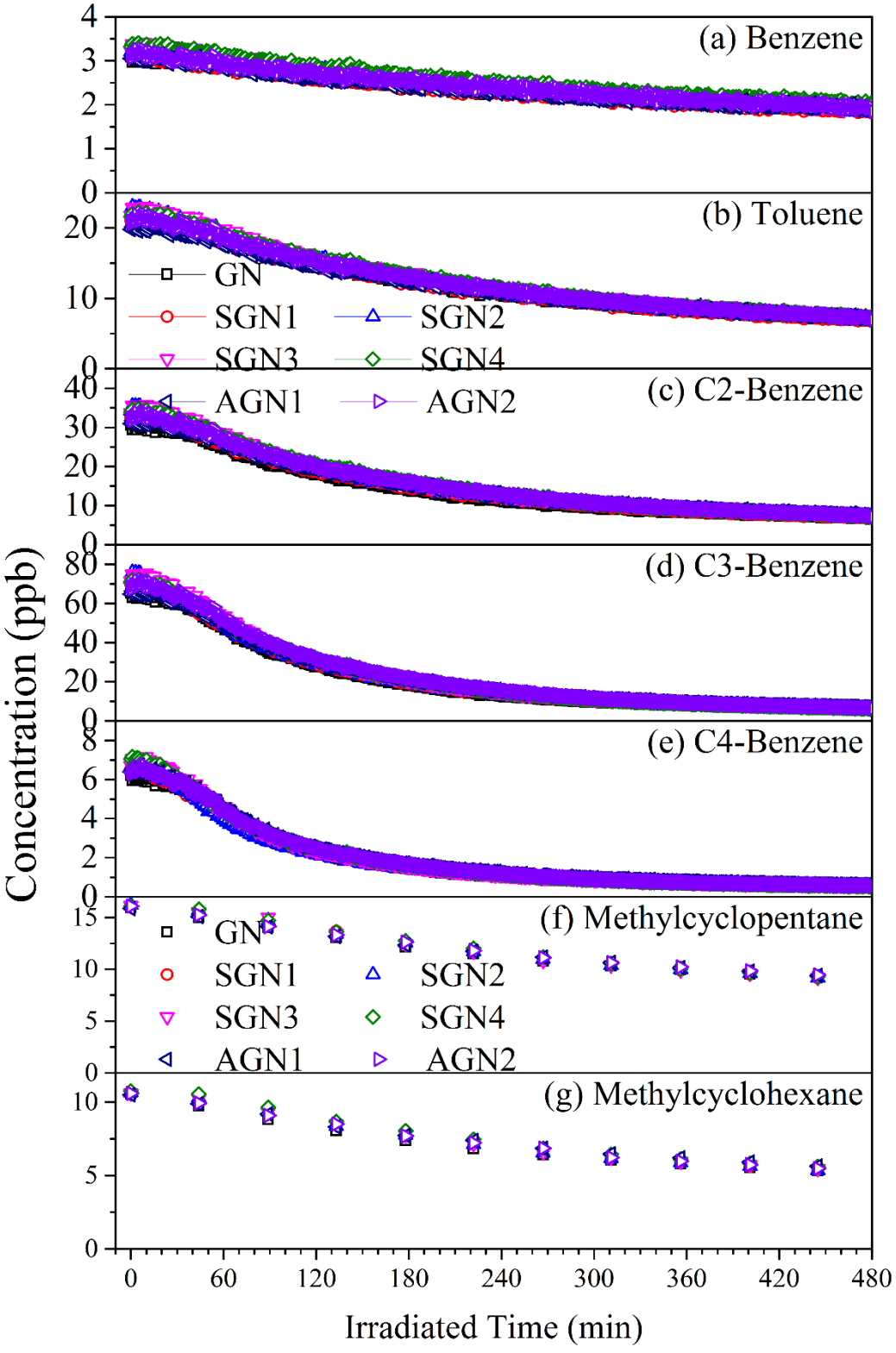

Fig. S3. Time variations of organic gas-phase species (a) Benzene, (b) Toluene, (c) C2-Benzene, (d) C3-Benzene, (e) C4-Benzene, (f) Methylcyclopentane, and (g) Methylcyclohexane in photo-oxidation of gasoline/NO_x in the presence or absence of SO_2 and NH_3. Letters in abbreviations represent the reactants introduced into the chamber reactor, i.e., "G" represents gasoline, "N" represents nitrogen oxides, "S" represents sulfur dioxide, "A" represents ammonia.

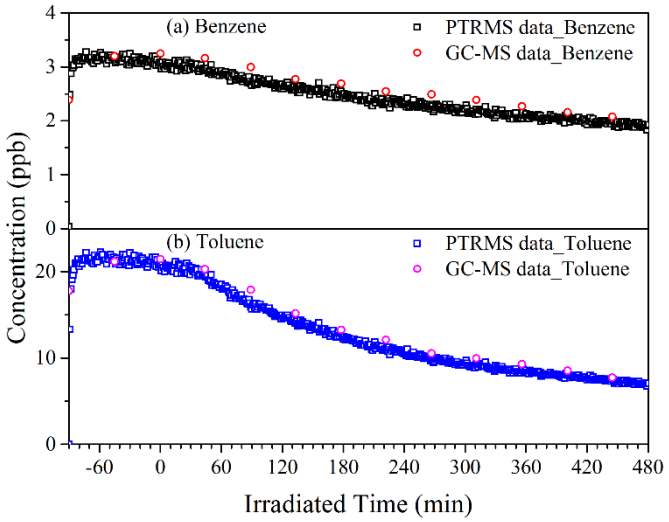

Fig. S4. Time variations of (a) Benzene and (b) Toluene measured by PTR-TOF and GC-MS during a typical chamber experiment (experiment GN).

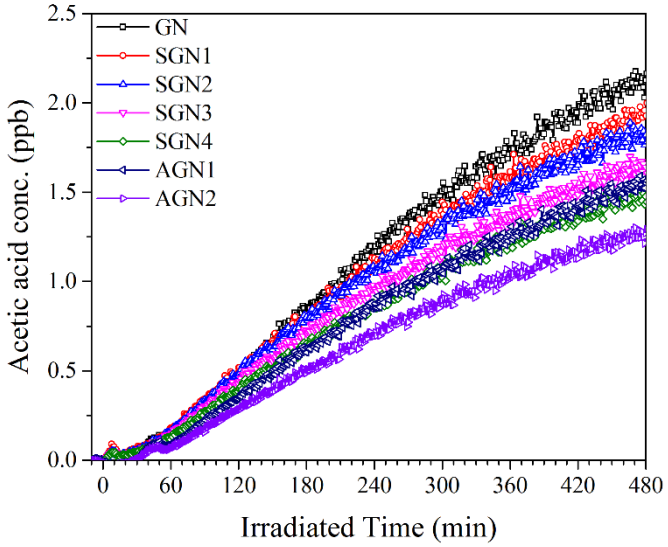

Fig. S5. Time variations of acetic acid during the photo-oxidation of gasoline/NO_x in the presence or absence of SO_2 and NH_3. Letters in abbreviations represent the reactants introduced into the chamber reactor, i.e., "G" represents gasoline, "N" represents nitrogen oxides, "S" represents sulfur dioxide, "A" represents ammonia.

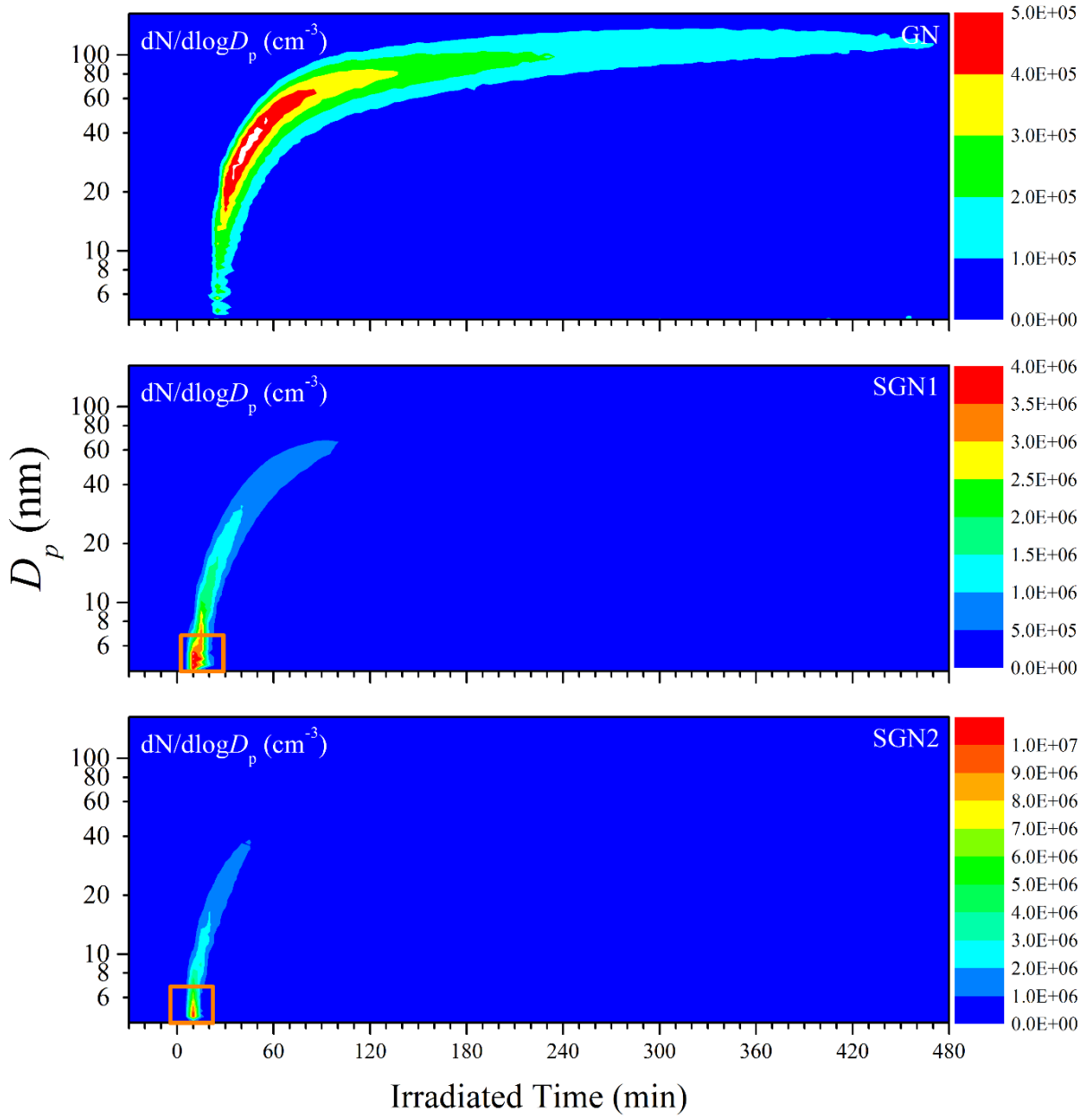

Fig. S6. Time series of the smaller size distributions (4−160 nm) derived from SMPS equipped with a nanometer differential mobility analyzer (Nano-DMA) for the generated secondary aerosol during the photo-oxidation experiments with different SO_2 concentrations.

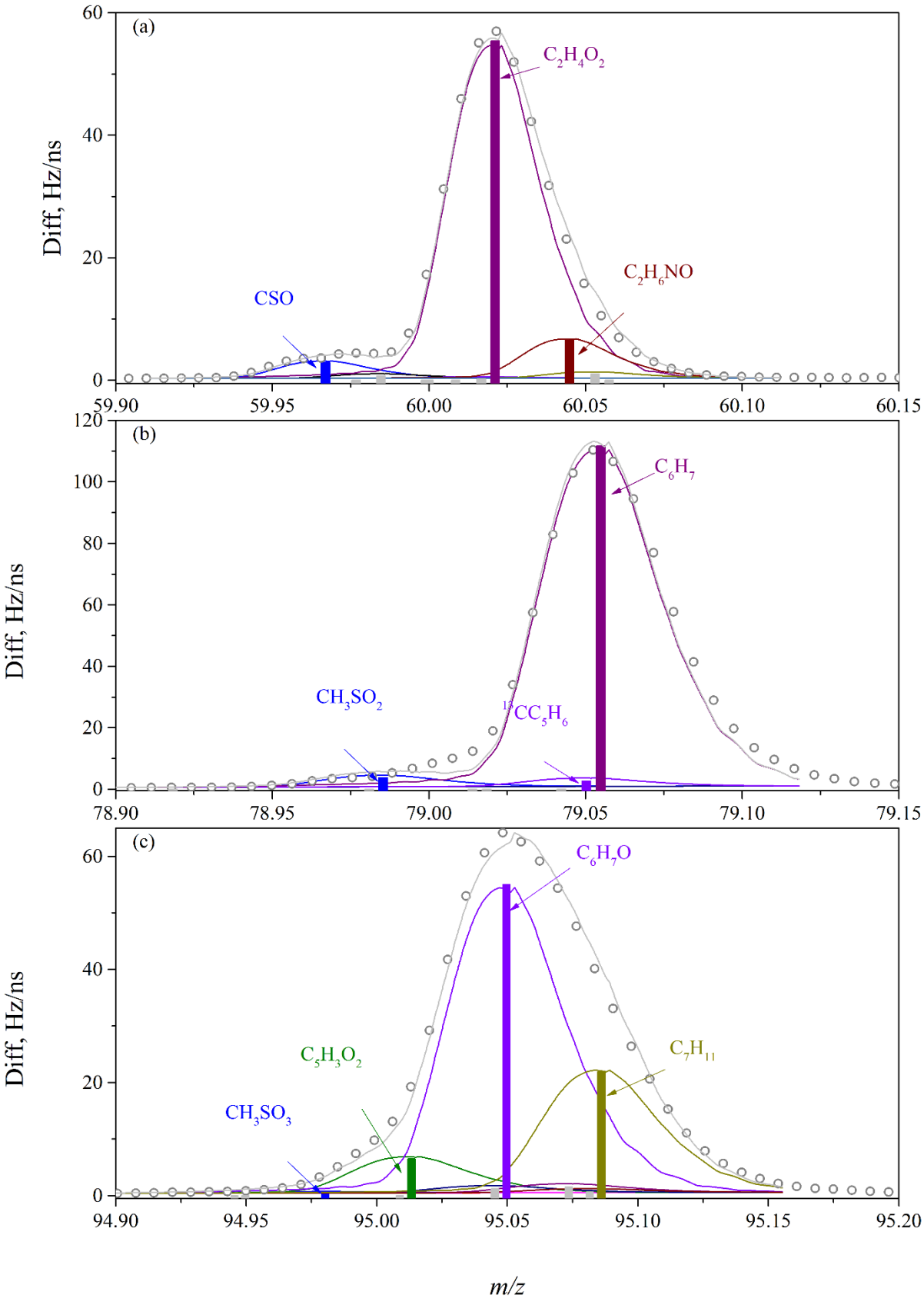

Fig. S7. Fitted peaks of average W-mode mass spectrum of organosulfur compounds (OS), (a) CSO^+, (b) $CH_3SO_2^+$, (c) $CH_3SO_3^+$.

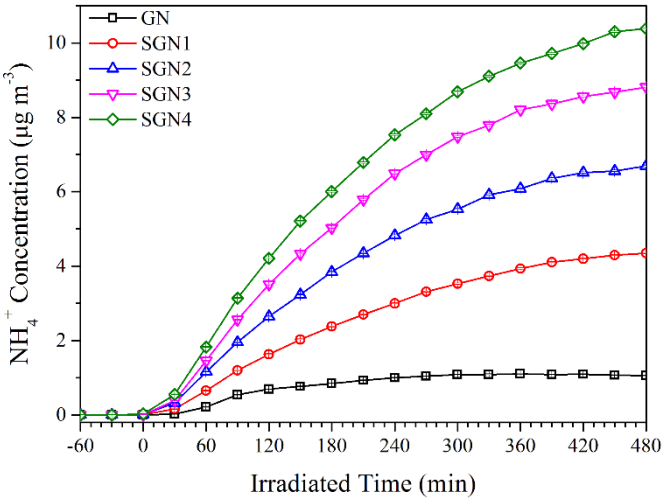

121

122 Fig. S8. Time series of the ammonium aerosol formed during the photo-oxidation experiments with different SO_2

123 concentrations without adding additional gaseous NH_3 (i.e., GN, SGN1, SGN2, SGN3 and SGN4 listed in Table S2).

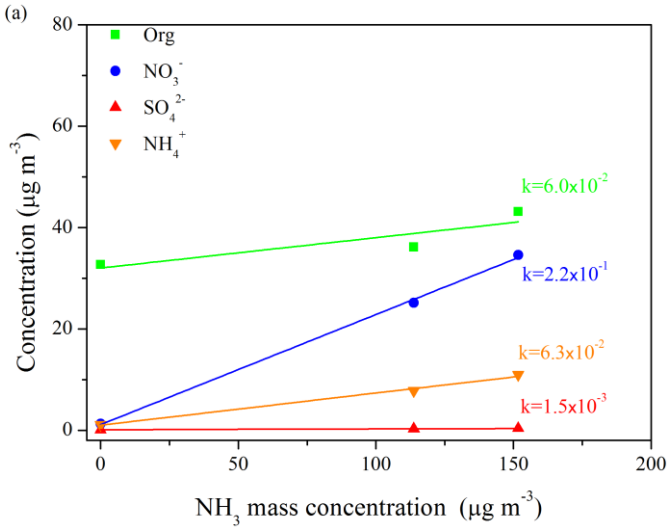
(a)
Org
NO3-
SO4 2-
NH4+
k=6.0x10-2
k=2.2x10-1
k=6.3x10-2
k=1.5x10-3
Concentration (μg m-3)
NH3 mass concentration (μg m-3)

124

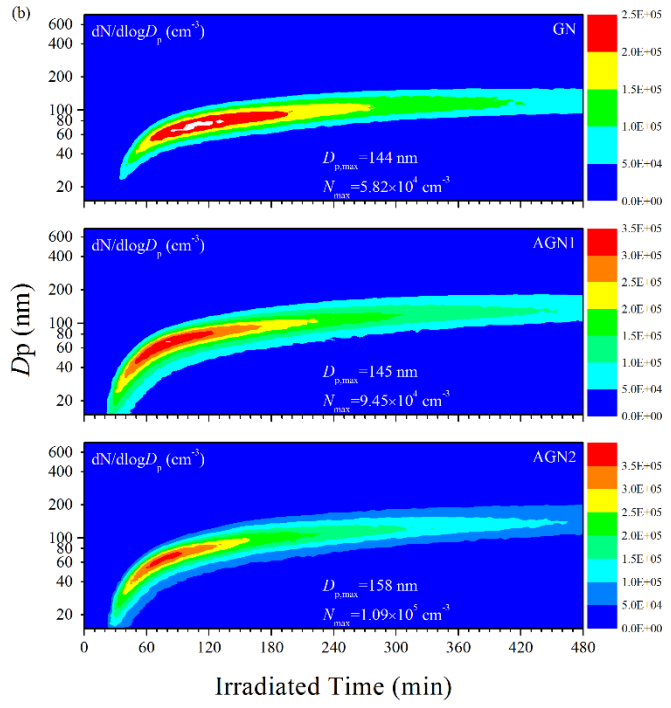
(b)
dN/dlogDp (cm-3)
GN
Dp,max=144 nm
Nmax=5.82×10⁴ cm-3
AGN1
Dp,max=145 nm
Nmax=9.45×10⁴ cm-3
AGN2
Dp,max=158 nm
Nmax=1.09×10⁵ cm-3
Dp (nm)
Irradiated Time (min)

125

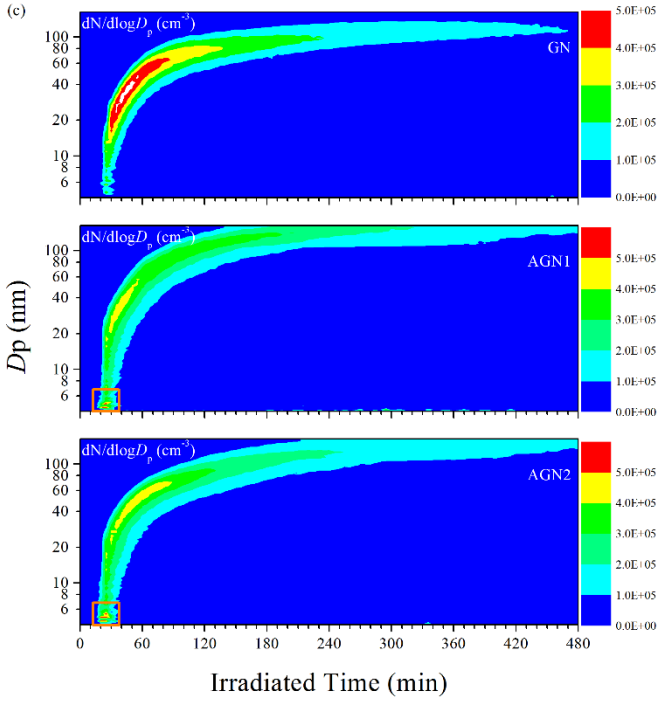

Fig. S9. (a) Linear relationship between the concentration of chemical species and NH_3 under different NH_3 initial concentration conditions. Each line (green (organic), blue (nitrate), red (sulfate), and orange (ammonium)) represents a linear fitting and the k values are the corresponding slopes for each chemical species. (b) Time series of the size distributions (20−700 nm) for the secondary aerosol generated during the photo-oxidation experiments with different NH_3 concentrations. $D_{p,max}$ and N_{max} represent the maximal diameter and number concentration of generated secondary aerosol, respectively, during each photo-oxidation experiment. (c) Time series of the smaller size distributions (4−160 nm) derived from SMPS equipped with a nanometer differential mobility analyzer (Nano-DMA) for the generated secondary aerosol during the photo-oxidation experiments with different NH_3 concentrations.

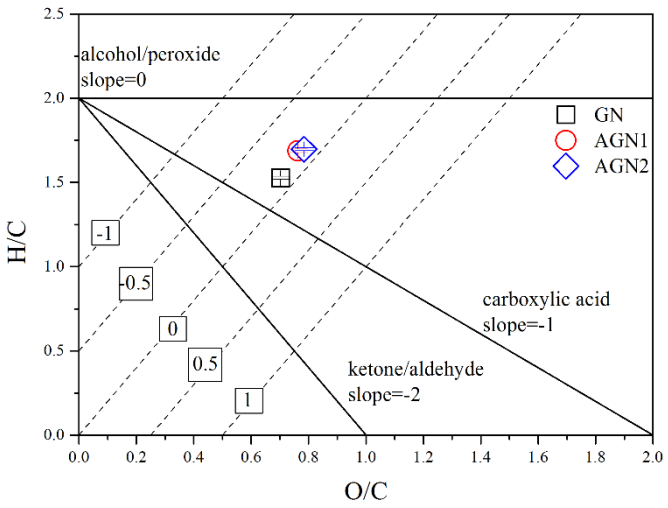

135

136 Fig. S10. Average O/C and H/C in SOA formed from the photo-oxidation of gasoline vapor at different concentrations of NH_3

137 (Exps. GN, AGN1 and AGN2).

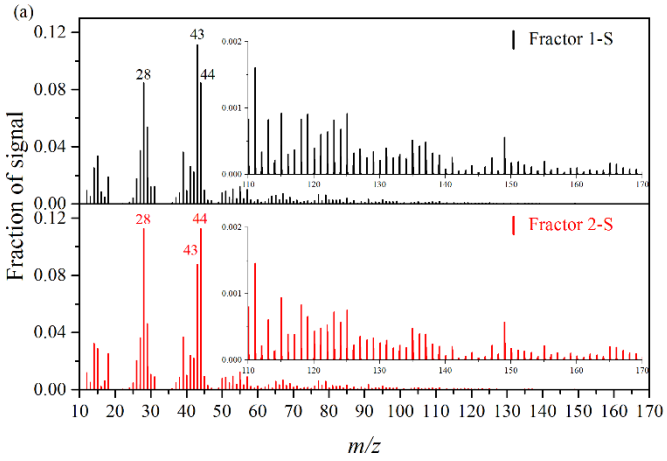

138

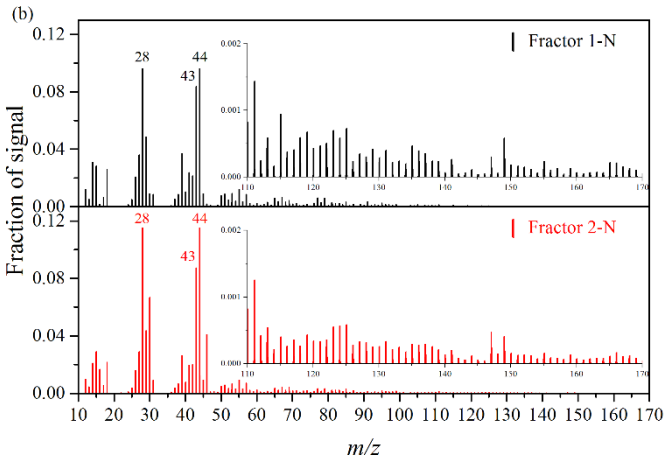

139

140 Fig. S11. Mass spectra of the two factors identified from the PMF analysis to the AMS data derived from the experiments at

141 different concentrations of (a) SO_2 (Exp. GN, SGN1, SGN2, SGN3 and SGN4) and (b) NH_3 (Exp. GN, AGN1 and AGN2).

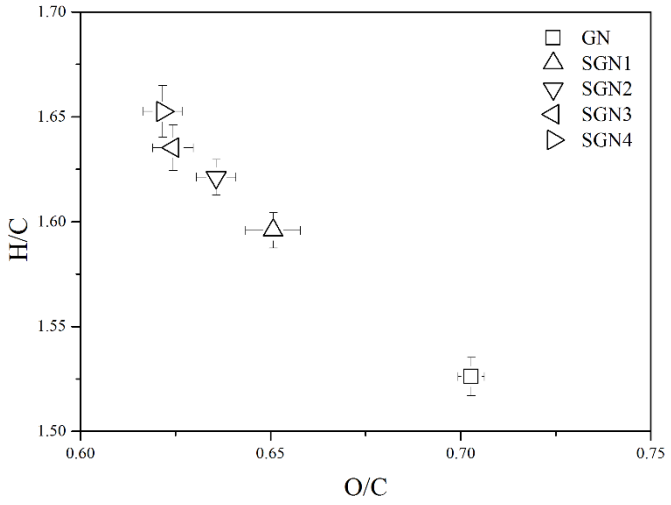

142

143 Fig. S12. Average O/C and H/C in SOA formed from the photo-oxidation of gasoline vapor at different concentrations of SO_2

144 (Exp. GN, SGN1, SGN2, SGN3 and SGN4).

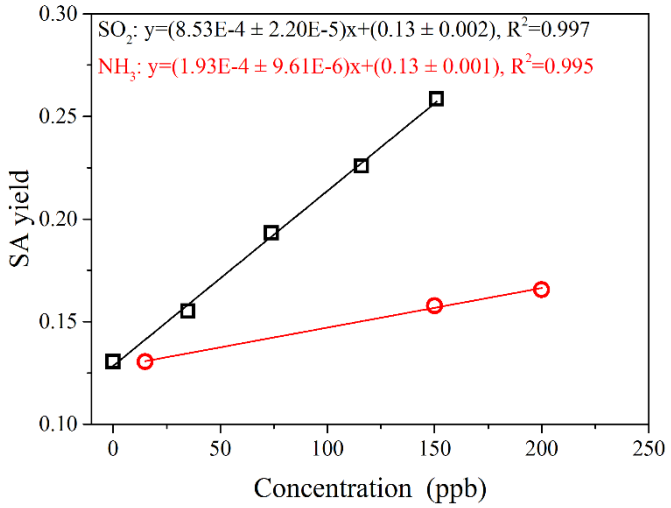

145

146 Fig. S13. Linear relationship between the concentration of SO_2 (or NH_3) and the SA yield.

References

DeCarlo, P. F., Slowik, J. G., Worsnop, D. R., Davidovits, P., and Jimenez, J. L.: Particle morphology and density characterization by combined mobility and aerodynamic diameter measurements. Part 1: Theory, Aerosol Sci. Tech., 38, 1185-1205, doi: 10.1080/027868290903907, 2004.

Liu, P. S. K., Deng, R., Smith, K. A., Williams, L. R., Jayne, J. T., Canagaratna, M. R., Moore, K., Onasch, T. B., Worsnop, D. R., and Deshler, T.: Transmission efficiency of an aerodynamic focusing lens system: Comparison of model calculations and laboratory measurements for the Aerodyne Aerosol Mass Spectrometer, Aerosol Sci. Tech., 41, 721-733, doi: 10.1080/02786820701422278, 2007.

Liu, Y., Li, S. M., and Liggio, J.: Technical Note: application of positive matrix factor analysis in heterogeneous kinetics studies utilizing the mixed-phase relative rates technique, Atmos. Chem. Phys., 14, 9201-9211, doi: 10.5194/acp-14-9201-2014, 2014.

Loza, C. L., Chhabra, P. S., Yee, L. D., Craven, J. S., Flagan, R. C., and Seinfeld, J. H.: Chemical aging of m-xylene secondary organic aerosol: laboratory chamber study, Atmos. Chem. Phys., 12, 151-167, doi: 10.5194/acp-12-151-2012, 2012.

Matsunaga, A., and Ziemann, P. J.: Gas-wall partitioning of organic compounds in a teflon film chamber and potential effects on reaction product and aerosol yield measurements, Aerosol Sci. Tech., 44, 881-892, doi: 10.1080/02786826.2010.501044, 2010.

McMurry, P. H., and Grosjean, D.: Gas and aerosol wall losses in Teflon film smog chambers, Environ. Sci. Technol., 19, 1176-1182, doi: 10.1021/es00142a006, 1985.

McMurry, P. H., and Rader, D. J.: Aerosol wall losses in electrically charged chambers, Aerosol Sci. Tech., 4, 249-268, doi: 10.1080/02786828508959054, 1985.

Paatero, P., and Tapper, U.: Positive matrix factorization: a non-negative factor model with optimal

169 utilization of error estimates of data values, Environmetrics, 5, 111-126, doi: 10.1002/env.3170050203,
170 1994.

171 Paatero, P.: Least squares formulation of robust non-negative factor analysis, Chemom. Intell. Lab.
172 Syst., 37, 23-35, doi: 10.1016/S0169-7439(96)00044-5, 1997.

173 Takegawa, N., Miyazaki, Y., Kondo, Y., Komazaki, Y., Miyakawa, T., Jimenez, J. L., Jayne, J. T.,
174 Worsnop, D. R., Allan, J. D., and Weber, R. J.: Characterization of an Aerodyne aerosol mass
175 spectrometer (AMS): intercomparison with other aerosol instruments, Aerosol Sci. Tech., 39, 760-770,
176 doi: 10.1080/02786820500243404, 2005.

177 Ulbrich, I. M., Canagaratna, M. R., Zhang, Q., Worsnop, D. R., and Jimenez, J. L.: Interpretation
178 of organic components from positive matrix factorization of aerosol mass spectrometric data, Atmos.
179 Chem. Phys., 9, 2891-2918, doi: 10.5194/acp-9-2891-2009, 2009.

180 Zhang, Q., Jimenez, J. L., Canagaratna, M. R., Ulbrich, I. M., Ng, N. L., Worsnop, D. R., and Sun,
181 Y.: Understanding atmospheric organic aerosols via factor analysis of aerosol mass spectrometry: a
182 review, Anal. Bioanal. Chem., 401, 3045-3067, doi: 10.1007/s00216-011-5355-y, 2011.

183 Zhang, X., Cappa, C. D., Jathar, S. H., McVay, R. C., Ensberg, J. J., Kleeman, M. J., and Seinfeld,
184 J. H.: Influence of vapor wall loss in laboratory chambers on yields of secondary organic aerosol, Proc.
185 Natl. Acad. Sci. USA, 111, 5802-5807, doi: 10.1073/pnas.1404727111, 2014.